Modelling Simul. Mater. Sci. Eng. **8** (2000) 871–879. Printed in the UK PII: S0965-0393(00)16191-1

Simulations of the initial transient during directional solidification of multicomponent alloys using the phase field method

U Grafe, B Böttger, J Tiaden and S G Fries
ACCESS e.V., Intzestraße 5, D-52056 Aachen, Germany

Received 2 March 2000, accepted for publication 30 July 2000

Abstract. This paper presents simulations of directional solidification of multicomponent alloys using the phase field method. In order to calculate thermodynamic quantities of the alloy, the phase field model has been coupled to multicomponent thermodynamic databases in an 'online' mode using the TQ-Interface of the software Thermo-Calc. Simulations of directional solidification of several alloys from the Ni–Al–Cr–Co–Ti system are presented for different pulling speeds. The results predict oscillations of the solidification velocity and the element concentrations evolving in the course of the initial transient as has been analytically shown for binary systems. In multicomponent systems these oscillations not only depend on the pulling speed but also on alloy composition.

1. Introduction

During the past few years, the phase field method has become an increasingly powerful tool for simulating solidification and solid-state transformations. The simulated morphologies become more and more complex while the simulated domains become larger, thus allowing one to study the physical effects in greater detail. For this purpose models employing multiple-order parameters have been developed which enable one to address phase transformations with more than two phases being involved [1–3]. In these simulations mainly binary systems are the target, employing an ideal solution model or a simplified approach for dilute multicomponent systems [4]. For instance, isothermal free dendritic growth in a binary system was simulated in [5, 6] and constrained dendritic growth in [4, 7, 8].

In contrast, the work presented in this paper primarily addresses systems of complex thermodynamics rather than complex morphologies. The model used here [9, 10] is capable of treating multiphase and multicomponent systems. In order to ensure the use of experimentally validated thermodynamic data within the phase field simulations, the model has been coupled with thermodynamic databases. The code has been interfaced to the software Thermo-Calc [11] via the TQ-Interface which offers a set of FORTRAN routines to calculate chemical potentials, molar Gibbs energies and phase equilibrium data. Moreover, the multicomponent diffusion matrix can be obtained by a subroutine of the software Dictra [12], which models the diffusivities as the product of atomic mobilities and thermodynamic factors. Mobility data are taken from databases and the thermodynamic factors are also calculated using Thermo-Calc. However, this feature of the model is more important for the simulation of solid-state transformations, while for the solidification simulations presented in this paper diffusion in

0965-0393/00/060871+09$30.00

the solid can be neglected. For all thermodynamic calculations the database described in [13] is used.

The purpose of this work is to investigate the segregation behaviour during directional solidification of alloys from the quinary Ni–Al–Co–Cr–Ti system at low solidification velocities. Benchmark tests with the software Dictra, which can be used to simulate phase transformations in isothermal one-dimensional calculation domains, prove the right growth kinetics and the correct tielines at the phase boundary [9, 10]. Simulations for modified alloy compositions have been carried out starting with a binary Ni–Al alloy and moving to the quaternary compositions.

2. The model

The multiphase field model has been described in detail elsewhere [1, 2, 10]. The evolution of the phase field ϕ_i for a phase i with respect to time is given by

$$\dot{\phi}_i = \sum_j^N \mu_{ij} \left[\sigma_{ij} \left(\phi_i \nabla^2 \phi_j - \phi_j \nabla^2 \phi_i + \frac{36}{\eta_{ij}^2} \phi_i \phi_j (\phi_i - \phi_j) \right) + \frac{6}{\eta_{ij}} \phi_i \phi_j \cdot \Delta G_{ij}^{\text{bulk}} \right] \tag{1}$$

where μ_{ij} is the mobility, η_{ij} is the interfacial energy, η_{ij} is the interface thickness, N is the number of phases, and $\Delta G_{ij}^{\text{bulk}}$ is the change in bulk Gibbs energy for the transformation of phase i to j. In these simulations only two phases are considered. Phase i stands for the primary γ phase while j represents the liquid phase. In the sharp interface limit this phase field equation models the normal velocity v_{n} of the interface between phases i and j

$$v_{\text{n}} = \mu_{ij} \left(\Delta G_{ij}^{\text{interface}} + \Delta G_{ij}^{\text{bulk}} \right) \tag{2}$$

where $\Delta G_{ij}^{\text{interface}}$ represents the product of the interfacial energy σ_{ij} and the curvature κ. The Gibbs energy difference of the bulk phases $\Delta G_{ij}^{\text{bulk}}$ is given by [14]

$$\Delta G_{ij}^{\text{bulk}} = G_j^{\text{molar}} \left(c_j^k \right) - \sum_{k=1}^{n} c_j^k \mu_i^k (c_i^k) \tag{3}$$

where c_i^k is the concentration, i.e. mole fraction of component k in phase i, μ_i^k is the chemical potential of component k in phase i, and G_j^{molar} is the molar Gibbs energy of phase j. This expression is calculated using the FORTRAN interface to Thermo-Calc (TQ-Interface) for the grid points within the diffuse interface. The phase field equations for a system containing N phases are coupled to the diffusion equations for each solute k

$$\dot{c}^k(\vec{x}, t) = \nabla \cdot \left(\sum_{i=1}^{N} \phi_i j_i^k \right) \tag{4}$$

where c^k is the mixture composition that varies across the diffuse interface from the concentration in one phase to the concentration in the other phase. In general, the diffusional flux j_i^k of a component k in phase i can be calculated according to the Fick–Onsager equation

$$j_i^k = - \sum_{l=1}^{n-1} \boldsymbol{D}_i^{kl} \nabla c_i^l. \tag{5}$$

The model is interfaced to the software Dictra to calculate the diffusion matrix $\boldsymbol{D}_i^{kl}$ for a phase i.

Table 1. Calculated liquidus and solidus temperatures and the solidification intervals of the investigated alloys.

	Ni–Al 21	Ni–Cr 21	Ni–Al 21 Cr 7	Ni–Al 21 Co 7 Cr 7	Ni–Al 21 Co 11 Cr 7	Ni–Al 21 Co 9 Cr 9	Ni–Al 15 Co 11 Cr 9 Ti 6
T^{liq}	1670.1	1696.1	1634.1	1628.4	1626.4	1617.0	1604.0
T^{sol}	1654.0	1693.6	1610.9	1595.2	1548.8	1538.3	1579.7
ΔT_0	16.1	2.5	23.2	33.2	79.5	78.7	24.3

3. Simulations of directional solidification

To examine the impact of the phase diagram on segregation profiles and the velocity of the solidification, front simulations of the initial transient during Bridgman-type solidification have been carried out for two different pulling speeds and different alloy compositions. Since for the liquid phase in the quaternary Ni–Al–Co–Cr system no reliable diffusion data are available, the diffusion coefficients are assumed to be constant at 10^{-9} m^2 s^{-1}. The diffusion coefficients in the solid were estimated from Dictra calculations in the Ni–Al–Cr system at liquidus temperature using the mobility database created by [15]. However, solidification calculations using these diffusivities show that diffusion in the solid has no significant impact on the results.

Simulations have been carried out for the two pulling speeds $v_{\mathrm{p1}} = 0.5$ μm s^{-1} and $v_{\mathrm{p2}} = 4.5$ μm s^{-1} at a constant temperature gradient $G = 11.1$ K mm^{-1}. A sample of the superalloy CMSX-4 that contains 10 elements when processed with pulling speed v_{p1} showed a planar front at the same gradient. Therefore it is likely that a planar front will be stable for all alloy compositions. In order to give a rough estimate with respect to front stability for the second pulling speed, v_{p2}, the criterion for the presence of constitutional undercooling in a binary alloy with linearized solidus and liquidus lines is used:

$$v_{\mathrm{c}} = GD/\Delta T_0 \tag{6}$$

where v_{c} is the critical solidification velocity for the stability of a planar front, ΔT_0 is the solidification interval and D is the diffusion coefficient in the liquid. This is derived for steady-state conditions with a maximum difference between the solid and liquid concentration at the interface. Thus the critical velocity estimated using equation (6) yields the lowest possible velocity at which an interface can become unstable. The solidification interval has been thermodynamically calculated, evaluating the liquidus and solidus temperatures in the multicomponent system (see table 1; the compositions are given in at%).

Applying this criterion for the second pulling speed would predict an unstable interface in contrast to v_{p1} for steady-state conditions. On the other hand, during the initial transient the pile-up or sink of solute is not fully developed and the front may remain morphologically stable for some time. However, even if the front is unstable, the one-dimensional simulations show an interesting effect.

3.1. Variation of the pulling speed

Figures 1 and 2 show the solidification velocity as a function of time for different Ni-based alloys and pulling speeds. It is obvious that for Ni–Al 21 the simulation for the higher pulling speed shows a slight oscillation of the solidification velocity during the initial transient, as well as for the concentration of Al in the solid as shown in figures 3 and 4. The higher solidification

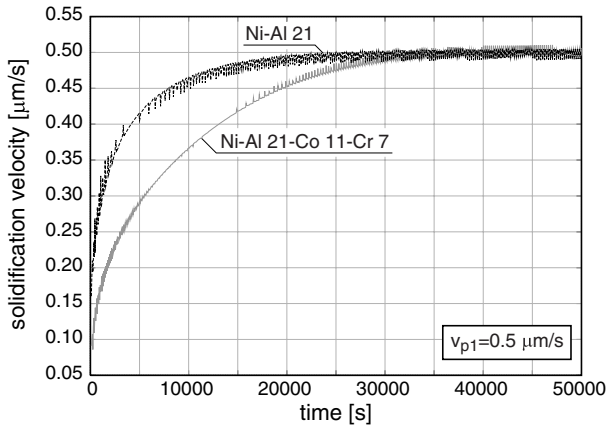

Figure 1. Solidification velocities as a function of time for two alloys during the initial transient with pulling speed of the Bridgman furnace $v_{p1} = 0.5\ \mu\text{m s}^{-1}$. The fine oscillations of both curves are due to numerical discretization and vanish using a finer grid resolution.

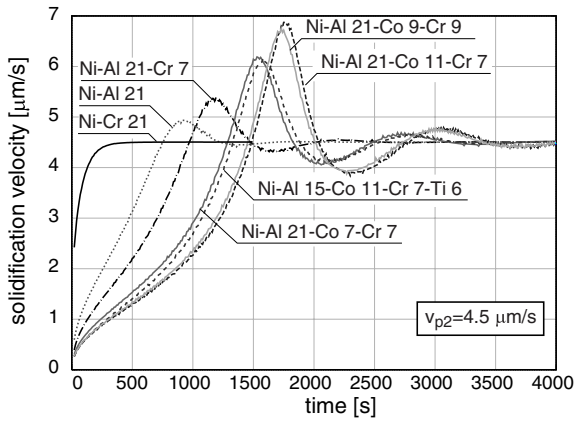

Figure 2. Solidification velocities as a function of time for different alloy compositions during the initial transient with pulling speed of the Bridgman furnace $v_{p2} = 4.5\ \mu\text{m s}^{-1}$.

velocity causes the front to segregate more solute and thereby shifts the solid concentrations to higher values than in the steady state. In this region of the phase diagram the partition coefficient is constant ($k = 0.951$) and thus the oscillation is not an effect of thermodynamics but results from the increased pulling speed. Such oscillations have been predicted in [16], which showed that the position of the solidification front in a reference frame moving at pulling speed approaches the fixed point of the steady state in an oscillatory way. This means that the diffusion length causes a damping effect since it does not adjust quickly enough to a modified solidification velocity. An indication of such an oscillation of the solidification velocity is given in [17, 18], in which an experiment of directional solidification under microgravity was carried out. During the initial transient, a binary transparent organic analogue showed an unstable solidification front at first, which changed to a planar front for a certain length of time and then became unstable again.

Figure 5 shows the result of the simulation of the quaternary alloy Ni–Al 21–Co 11–Cr 7. The segregation profiles of the elements Al, Co and Cr are plotted for pulling speed v_{p1}.

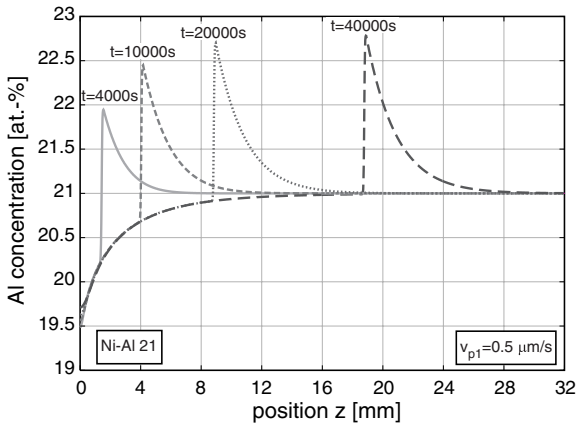

Figure 3. Concentration profile of Al in the binary alloy Ni–Al 21 for the liquid and solid phases at different times during the initial transient of one-dimensional directional solidification. The pulling velocity is $v_{\mathrm{p1}} = 0.5\ \mu\mathrm{m\ s}^{-1}$.

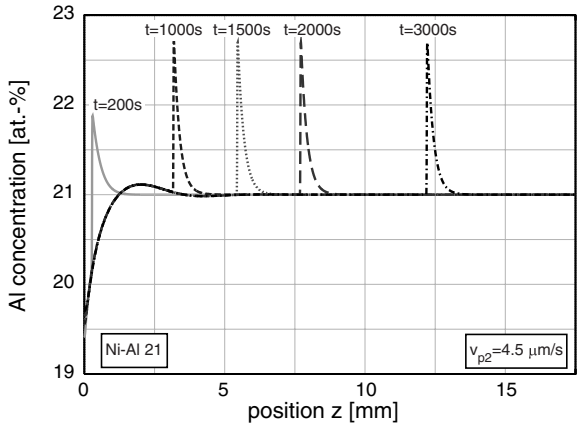

Figure 4. Concentration profile of Al in Ni–Al 21 in the liquid and solid phases at a pulling velocity of $v_{\mathrm{p2}} = 4.5\ \mu\mathrm{m\ s}^{-1}$ for different times during the initial transient of one-dimensional directional solidification.

The solidification velocity as a function of time, which is shown in figure 1, does not reveal oscillatory behaviour. The segregation behaviour of Cr during the initial transient is particularly noticeable. For this alloy the initial equilibrium concentrations of Cr in the solid and the liquid are almost of the same value, i.e. the partition coefficient is equal to unity. This value is shifted due to the beginning segregation of Al and Co, which leads to an increase in the equilibrium concentration of Cr in the solid. With ongoing solidification the partition coefficient becomes smaller than unity. At the later stage of the initial transient the solid concentration falls again towards its initial value of 7 at%. It can be concluded, therefore, that during the initial transient of directional solidification in a multicomponent system the chemical interactions of all elements can lead to deviations from the segregation behaviour that we know from binary systems.

Figure 6 presents the corresponding concentration profiles for pulling speed v_{p2}. The segregation behaviour is basically of the same nature, but the solid and the liquid concentrations

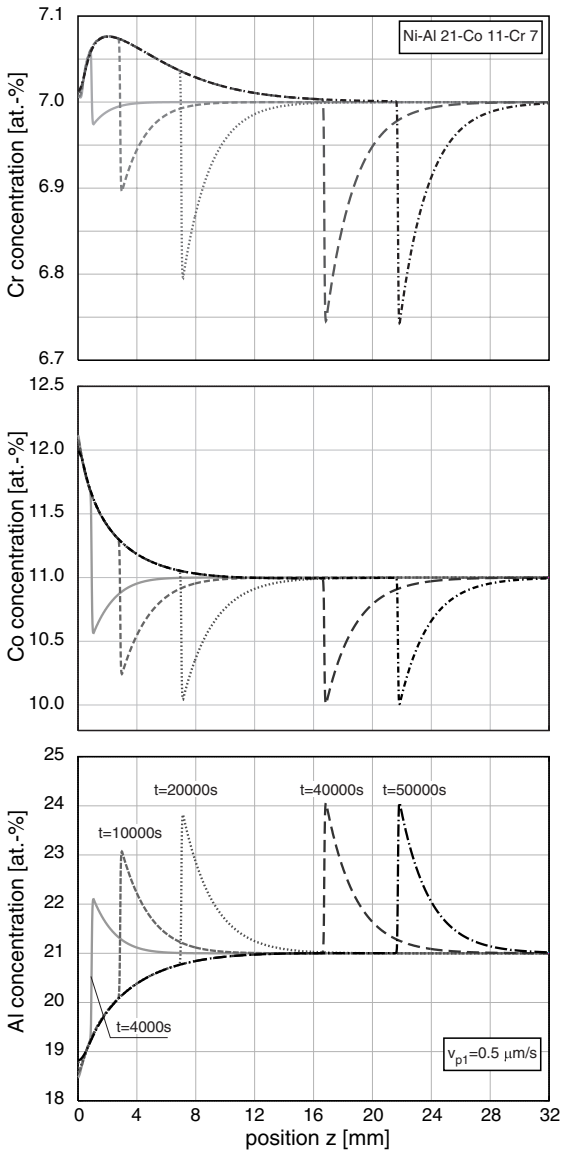

Figure 5. Concentration profiles for Al, Co and Cr of the alloy Ni–Al 21–Co 11–Cr 7 in the liquid and solid phases for different times during the initial transient of one-dimensional directional solidification. The pulling velocity is $v_{\mathrm{p1}} = 0.5\ \mu\mathrm{m\ s}^{-1}$.

of all the elements oscillate. The oscillation of the solidification velocity is also illustrated in figure 2. Compared to the binary alloy Ni–Al 21, the amplitude of the oscillation is higher.

3.2. Variation of alloy composition

Figure 7 presents the segregation profiles of the quaternary alloy Ni–Al 21–Co 7–Cr 7 with a reduced Co concentration compared to Ni–Al 21–Co 11–Cr 7. This change in composition now leads to a lower concentration of Cr in the solid compared to the liquid phase. As a

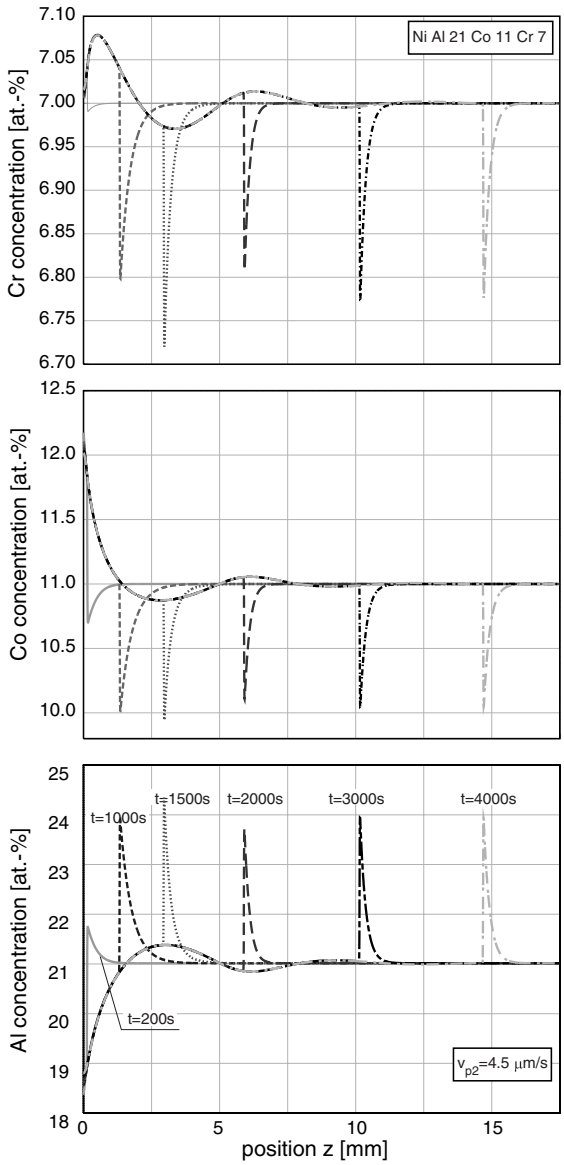

Figure 6. Concentration profiles for Al, Co and Cr of the same alloy as figure 5 (Ni–Al 21–Co 11–Cr 7) in the liquid and solid phases for different times during the initial transient of one-dimensional directional solidification. The pulling velocity is $v_{p2} = 4.5\ \mu\mathrm{m\ s}^{-1}$.

consequence, an initial pile-up ahead of the solidification front turns to a sink in the later stage of the initial transient. Compared to the alloy Ni–Al 21–Co 11–Cr 7, the oscillations of the Cr concentration profile are less pronounced. This behaviour can be related to the oscillation of the solidification velocity, which also reveals a lower amplitude; see figure 2. The amplitude of the oscillations of the profiles for Al and Co, which are not presented here, is also lower.

The solidification velocities as a function of time for additional alloy compositions from the system Ni–Al–Co–Cr-Ti are presented in figure 2. Comparing the curves of the binary

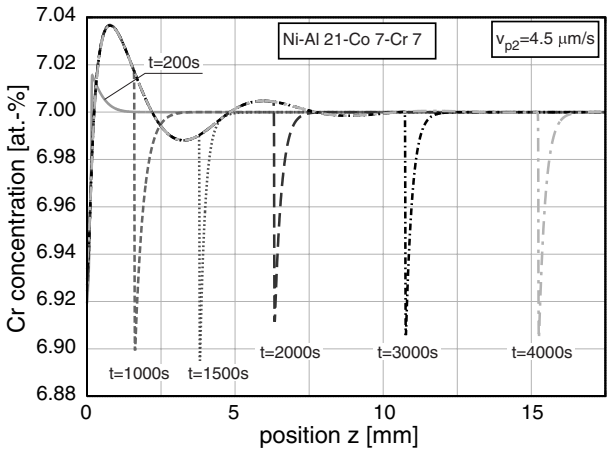

Figure 7. Concentration profiles for Cr in the liquid and solid phases of the alloy Ni–Al 21–Co 7–Cr 7 during the initial transient of one-dimensional directional solidification. The Co content is lowered to 7% compared to the alloy presented in figure 6. The pulling velocity is $v_{p2} = 4.5\,\mu\mathrm{m\,s^{-1}}$.

Ni–Al 21, Ni–Cr 21, the ternary Ni–Al 21–Cr 7, and the quaternary alloys Ni–Al 21–Co 7–Cr 7, Ni–Al 21–Co 11–Cr 7, it becomes obvious that the slope of the curves in the stage before the oscillations occur is lower with increasing alloy composition and solidification interval. This means that movement of the solid–liquid interface becomes more retarded with increasing content of foreign atoms. Moreover, the solidification velocities with the lowest slope in the beginning show the highest amplitude of the oscillations during the later stage of the initial transient.

Additional simulations for other alloy compositions have been carried out so that the total concentration of the alloying elements is set constant at the value of the alloy Ni–Al 21–Co 11–Cr 7. The solidification velocity of the alloy Ni–Al 15–Co 11–Cr 7–Ti 6 in which 6% Al is substituted by Ti increases more rapidly compared to Ni–Al 21–Co 11–Cr 7, figure 2. Obviously the substitution of Al with Ti makes the solid–liquid interface more mobile, although this composition contains an additional alloying element. The alloy Ni–Al 21–Co 9–Cr 9 with an increased Cr concentration and a decreased Co concentration shows a slight decrease in solidification velocity compared to Ni–Al 21–Co 11–Cr 7. The behaviour of these two alloys and the binary Ni–Cr 21, which does not show oscillatory behaviour, clarifies that the impact of the individual elements on solidification velocity is different.

Summarizing the analyses of the initial transient for the different alloy compositions it can be concluded that the solid–liquid interface becomes more retarded with increasing solidification interval and the addition of alloying elements, although the impact of the individual elements is different. Moreover, a more retarded interface during the first stage of the initial transient will show a higher amplitude of the oscillation later. The uncertainty of the diffusion coefficients in the liquid will also influence the equilibrium concentrations at the solid–liquid interface which has not been taken into account in these simulations. However, the impact of the pulling speed will be more important. Predictions for the solidification of multicomponent systems must be related to the evolution of the tielines and coupled to the phase transformation kinetics. For this, numerical simulation is a useful tool.

4. Summary

Simulations of the initial transient during directional solidification of multicomponent alloys predict that under diffusion controlled conditions oscillations of the solidification velocity during the initial transient are possible and will lead to oscillating concentrations in the solid. The amplitude of these oscillations not only increases with increasing pulling speed, but also depends on the thermodynamic characteristics of the alloy system under consideration, i.e. the evolution of the tielines between solid and liquid. A higher content of alloying elements retards a solid–liquid interface in the first stage, which in turn amplifies the oscillations in the later stage of the initial transient. In contrast to this, deviations in the evolution of concentration profiles in the solid from that observed in binary alloys can also be due to the evolution of the tielines during the initial transient instead of the oscillations of the solidification velocity. Predictions for multicomponent systems must take into account the thermodynamic properties of the alloy which couple back on kinetic effects. Further work could investigate these effects experimentally for different alloy compositions, especially under microgravity conditions to reduce convection in the liquid. Experimental results can then be compared with one- and two-dimensional phase field simulations predicting the segregation behaviour and the morphological stability of the interface.

Acknowledgments

The authors gratefully acknowledge the financial support of the Deutsche Forschungsgemeinschaft (DFG) within the research project SFB 370 'Integral Material Modelling'.

References

[1] Steinbach I, Pezzolla F, Nestler B, Seeßelberg M, Prieler R, Schmitz G J and Rezende J L L 1996 *Physica* D **94** 135–47
[2] Tiaden J, Nestler B, Diepers H J and Steinbach I 1998 *Physica* D **115** 73–86
[3] Chen L Q and Yang W 1994 *Phys. Rev.* B **50** 15 752–6
[4] Tiaden J, Grafe U and Böttger B 2000 *Proc. Euromat 99* vol 3, p 40f
[5] Warren J A and Boettinger W J 1995 *Acta Metall. Mater.* **43** 689–703
[6] McCarthy J F 1995 *Acta Metall. Mater.* **45** 4077–91
[7] Tiaden J and Grafe U 2000 *Proc. Int. Conf. on Solid-Solid Phase Transformations '99 (Kyoto, 1999)* ed M Koiwa, K Otsuka and T Miyasaki, pp 737–40
[8] Tiaden J 1999 *J Cryst. Growth* **198/199** 1275–80
[9] Grafe U, Böttger B, Tiaden J and Fries S G 2000 *Proc. Int. Conf. on Solid-Solid Phase Transformations '99 (Kyoto, 1999)* at press
[10] Grafe U, Böttger B, Tiaden J and Fries S G 2000 *Scr. Mater.* **42** 1179–86
[11] Sundman B, Jansson B and Anderson J O 1985 *Calphad* **2** 153–90
[12] Engström A, Höglund L and Ågren J 1994 *Metall. Trans.* **25a** 1127–34
[13] Saunders N 1996 *Superalloys 1996* ed R D Kissinger *et al* (Warrendale, PA: TMS) p 101
[14] Hillert M 1998 *Phase Equilibria, Phase Diagrams and Phase Transformations: A Thermodynamic Basis* (Cambridge: Cambridge University Press)
[15] Engström A and Ågren J 1996 *Z. Metallkunde* **87** 92–7
[16] Warren J A and Langer J S 1993 *Phys. Rev.* E **47** 2702–12
[17] Kauerauf B 1999 *PhD Thesis* ed P R Sahm (Shaker)
[18] Kauerauf B, Zimmermann G, Rex S, Mathes M and Grote F 2000 *J. Cryst. Growth* accepted